The Canadian Mineralogist
Vol. 54, pp. 539-553 (2016)
DOI: 10.3749/canmin.1400069

MINERALOGY AND ORIGIN OF EXSOLUTION IN Ti-RICH MAGNETITE FROM DIFFERENT MAGMATIC Fe-Ti OXIDE-BEARING INTRUSIONS

Wei TAN and Peng LIU

Key Laboratory of Mineralogy and Metallogeny, Guangzhou Institute of Geochemistry, Chinese Academy of Sciences, Kehua Street 511, Guangzhou 510640, China
University of Chinese Academy of Sciences, Beijing 100049, China

Hongping HE[§], Christina Y. WANG, and Xiaoliang LIANG

Key Laboratory of Mineralogy and Metallogeny, Guangzhou Institute of Geochemistry, Chinese Academy of Sciences, Kehua Street 511, Guangzhou 510640, China
Guangdong Provincial Key Laboratory of Mineral Physics and Materials, Guangzhou 510640, China

Abstract

Titanium-rich magnetite from different magmatic Fe-Ti oxide-bearing intrusions consists of host magnetite (nearly pure Fe_3O_4) and different types of exsolution. The exsolution of Ti-rich magnetite is indicative of the physical and chemical conditions at which the host intrusions formed. However, the mechanisms to form these types of exsolution have been debated. To examine the formation mechanisms of the different types of exsolution, multiple microanalytical techniques, such as electron microprobe analysis, micro Raman spectroscopy, and micro X-ray diffraction, were used to examine the chemical composition, morphology, and crystalline structure of exsolved minerals in Ti-rich magnetite from different Fe-Ti oxide-bearing intrusions in China. The characterization results indicate that pleonaste and ilmenite are the two dominant exsolution phases in the Ti-rich magnetite, whereas the ulvöspinel phase is barely found. The ilmenite exsolution may have different origins: (1) the cloth-texture lamellae primarily exsolved as ulvöspinel, which was oxidized to ilmenite later at $<$600 °C; (2) most of the trellis- and sandwich-type lamellae formed by "oxy-exsolution" at $>$600 °C; (3) some ilmenite lamellae exsolved directly from cation-deficient solid solution due to the substitution of $Ti^{4+} + \square \rightarrow 2Fe^{2+}$; (4) sub-solidus re-equilibration of coexisting Fe-Ti oxides can also lead to ilmenite exsolution in Ti-rich magnetite and magnetite exsolution in ilmenite.

Keywords: Ti-rich magnetite, ilmenite exsolution, magmatic Fe-Ti oxide-bearing intrusions.

Introduction

Titanium-rich magnetite commonly occurs in Fe-Ti oxide-bearing, mafic-ultramafic intrusions and anorthosite massifs (Pang *et al*. 2008, 2010, Wang *et al*. 2008, Zhao *et al*. 2009, Morisset *et al*. 2010, Song *et al*. 2013, Liu *et al*. 2015). The Ti-rich magnetite-ilmenite thermo-oxybarometer has been widely used to estimate both temperature and oxygen fugacity in igneous and metamorphic rocks (Buddington & Lindsley 1964). The textural and compositional features of Ti-rich magnetite are also potential indicators of the physical and chemical conditions of the magmas from which it crystallized (McConnell 1975, Price 1980, Reynolds 1985, Vongruenewaldt *et al*. 1985, Speczik *et al*. 1988).

Titanium-rich magnetite is supposed to be a spinel-type solid solution ($spinel_{ss}$, the subscript "ss" represents solid solution) with a theoretical formula of AB_2O_4, where the cations at site A are tetrahedrally coordinated (*e.g.*, Fe^{2+}, Fe^{3+}, and Mg^{2+}), and those at the B site are octahedrally coordinated (*e.g.*, Ti^{4+}, Cr^{3+}, $A1^{3+}$, Fe^{2+}, and Fe^{3+}). A minor amount of cationic vacancies ($\square$) can also be present in cation-deficient $spinel_{ss}$ (Collyer *et al*. 1988, Senderov *et al*. 1993, Lattard *et al*.1995, 2005, Zhou *et al*. 1999). $Spinel_{ss}$ in mafic-ultramafic intrusive rocks would

§ *Corresponding author e-mail address*: hehp@gig.ac.cn

experience intensive sub-solidus re-equilibration on slow cooling (Frost & Lindsley 1991), resulting in various types of exsolution in Ti-rich magnetite. The exsolved phases in Ti-rich magnetite are mainly composed of ilmenite ($FeTiO_3$), ulvöspinel (Fe_2TiO_4), and pleonaste ($Mg_xFe_{2-x}AlO_4$, $x = 0 \sim 2$). Ulvöspinel and pleonaste belong to the cubic system, whereas ilmenite belongs to the hexagonal system. The morphology and composition of the exsolved phases have been described in detail in previous studies (Ramdohr 1980, Haggerty 1991), however, some ultrafine exsolved phases with similar optical properties or chemical compositions, such as ulvöspinel/ilmenite and magnetite/hematite, are still difficult to clearly identify in practice (Ramdohr 1953, Price 1981, Krasnova & Krezer 1995, Charlier *et al*. 2007, Pang *et al*. 2008, Wang *et al*. 2008, Morisset *et al*. 2010). Therefore, characterization by micro analysis techniques, such as micro X-ray diffraction and micro Raman spectroscopy, is desired to provide important information about the ultrafine exsolved minerals.

The solvus of the pleonaste–magnetite solid solution (Ple–Mt_{ss}) lies below ~900 °C (Turnock & Eugster 1962) and that of the ulvöspinel–magnetite solid solution (Usp–Mt_{ss}) lies below ~600 °C (Vincent *et al*. 1957, Buddington & Lindsley 1964). The exsolution of ulvöspinel and pleonaste in Ti-rich magnetite is considered to result from the miscibility gap of the solid-solution series (Price 1980, 1981), but the origin of ilmenite exsolution in Ti-rich magnetite remains controversial (Buddington & Lindsley 1964, Lattard 1995, Krasnova & Krezer 1995, Mücke 2003). Synthetic experiments indicate that ilmenite exsolution can be formed by "oxy-exsolution" of stoichiometric Usp–Mt_{ss} (Buddington & Lindsley 1964) or by vacancy relaxation of cation-deficient titaniferous $spinel_{ss}$ (Lattard 1995). It seems that either process can uniquely explain the origin of the variable ilmenite exsolution in natural Ti-rich magnetite, which is formed under more complicated conditions than synthetic samples.

In this study, a combination of micro analysis techniques, including electron microprobe analysis (EMPA), micro X-ray diffraction, and micro Raman spectroscopy, were applied to characterize the composition, morphology, and crystalline structure of the exsolved phases in Ti-rich magnetite from four representative Fe-Ti oxide-bearing intrusions in China. The new data set enables us to examine the origin of different types of exsolution in Ti-rich magnetite, especially ilmenite exsolution, and reconstruct the original composition of the $spinel_{ss}$. This information has significant implications for understanding the sub-solidus re-equilibration of Ti-rich magnetite in Fe-Ti oxide-rich intrusions.

Sampling

Samples were collected from three mafic-ultramafic intrusions in China, the Bijigou, Panzhihua, and Xinjie intrusions, and from the Damiao anorthosite massif.

The Bijigou intrusion is located in the northern margin of the Yangtze Block (Central China). This intrusion, together with the Ni-Cu-(PGE) sulfide-bearing Wangjiangshan and Beiba intrusions, make up the Neoproterozoic Hannan mafic complex zone. The Bijigou intrusion is composed of a basal breccia zone with Cr-rich magnetite mineralization, a lower unit composed of pyroxenite with minor dunite, harzburgite, troctolite, and anorthosite, a middle unit of gabbro and gabbronorite with magnetite mineralization, and an upper unit of diorite (Zhou *et al*. 2002). The samples were collected from the middle unit.

The ~1.74 Ga Damiao complex in the North China Craton consists of anorthosite (85%), norite (10%), mangerite (4%), and minor troctolite (<1%). The Fe-Ti-P-rich oxide ore bodies are mainly hosted in anorthosite and leuconorite, and the ores are like nelsonite as seen elsewhere (Chen *et al*. 2013). The samples were collected from the Fe-Ti-P-rich oxide ore bodies.

The Panzhihua and Xinjie layered intrusions are part of the ~260 Ma Emeishan large igneous province in SW China. The Panzhihua intrusion, which is one of the most important Fe-Ti-V-rich oxide deposits in China, hosts up to 60 m-thick massive Fe-Ti oxide ore bodies at the base of the intrusion (Zhou *et al*. 2005). Two samples (PZH-I and PZH-II) were collected from this intrusion; the Ti-rich magnetite in the PZH-I sample coexists with sulfides in the interstitial phases, whereas the Ti-rich magnetite in the PZH-II sample mainly coexists with cumulus silicates (olivine, clinopyroxene, and plagioclase).

The Xinjie intrusion comprises a marginal zone and three units (Dong *et al*. 2013). Disseminated, Cr-rich Fe-Ti oxides occur in Units I and II, which are composed of ultramafic rocks such as wehrlite and clinopyroxenite, whereas Cr-poor Fe-Ti oxides make up several Fe-Ti oxide-rich layers in Unit III in the upper part of the intrusion (Dong *et al*. 2013). The samples were collected from the Fe-Ti oxide-rich layers and barren gabbro in Unit III.

Methods

Electron microprobe analysis

The BSE images of the samples and quantitative analyses of minerals were obtained using a JEOL JAX-8100 electron microprobe in the Guangzhou Institute of Geochemistry (GIG), Chinese Academy

of Sciences (CAS). Analyses were performed using an accelerating voltage of 15 kV and a beam current of 20 nA. X-ray matrix corrections were based on a routine ZAF method.

Micro X-ray diffraction

The Micro X-ray diffraction analyses were conducted with a Rigaku D/max Rapis IIR micro XRD system (at Central South University, China) operating at 40 kV and 250 mA (Cu$K\alpha$) and using X-ray exposures of 20–60 min. The X-ray beam (~100 μm diameter) was focused on the selected areas of the thin sections. The samples were rotated during measurement.

Raman spectroscopy

Raman spectra were obtained with a RM2000 laser Raman spectrometer at GIGCAS employing the 514.5 nm line of an Ar ion laser. The spectra were collected in the range of 100–1600 cm^{-1}. The reproducibility of peaks was checked with a silicon sample before examination. The laser power and acquisition time were carefully controlled to avoid laser-induced thermal effect and oxidation.

Results

Ilmenite exsolution

Ilmenite exsolution is generally divided into three types: (1) composite-type, ilmenite granules with scarce lamellae within or in the rim of host magnetite; (2) sandwich-type, thick ilmenite lamellae predominantly in one set of {111} planes; and (3) trellis-type, thin ilmenite lamellae in all {111} planes of the host magnetite (Buddington & Lindsley 1964, Haggerty 1991). The Ti-rich magnetite in the Bijigou intrusion exhibits typical composite-type ilmenite exsolution, which is denoted as $Ilmenite_B$ in this study (Fig. 1a). The Ti-rich magnetite in the Xinjie intrusion mainly contains sandwich-type and trellis-type ilmenite lamellae, denoted as $Ilmenite_{Xs}$ and $Ilmenite_{Xt}$, respectively (Fig. 1b). Note that the primary ilmenite coexisting with Ti-rich magnetite in the Xinjie intrusion contains various Fe-rich exsolutions (Fig. 1c). The Ti-rich magnetite in the Damiao complex has two types of ilmenite lamellae, including thick (20 to 100 μm) sandwich-type lamellae with vermicular pleonaste particles inside, denoted as $Ilmenite_{Ds}$ (Fig. 1d), and thin trellis-type lamellae (~10 μm) coexisting with pleonaste lamellae, denoted as $Ilmenite_{Dt}$ (Fig. 1e). The PZH-I Ti-rich magnetite also has sandwich-type lamellae (5 to 20 μm) with sparse vermicular pleonaste particles inside, denoted as $Ilmenite_{Ps}$ (Fig. 1f).

The ilmenite lamellae in this study contain lower TiO_2 contents than pure ilmenite (ω_{TiO2} = 52.64 wt.%). The ferrous and ferric iron contents of the ilmenite lamellae were estimated from stoichiometry and charge balance. The $Fe_2O_{3cal.}$ contents of the ilmenite lamellae in the Ti-rich magnetite of the Bijigou intrusion, Damiao complex, and Panzhihua intrusion (PZH-I) range from 0.01 to 3.0 wt.%, whereas the sandwich-type and trellis-type ilmenite lamellae in the Ti-rich magnetite of the Xinjie intrusion contain more than 10 wt.% $Fe_2O_{3cal.}$ (Table 1).

The ilmenite exsolutions in the Ti-rich magnetite from the different samples have similar Raman spectra (Fig. 2), exhibiting three indicative bands of pure ilmenite at *ca*. 681, 333, and 226 cm^{-1} (Table 2). Some extra weak Raman bands occur at *ca*. 600, 430, and 1370 cm^{-1}. These weak signals are similar to those of oxidized Ti-rich magnetite or titanomaghemite, but not identical to those for hematite or magnetite (Shebanova & Lazor 2003, Wang *et al*. 2004). As some of the ilmenite exsolution contains a minor amount of Fe^{3+} (Table 1), these weak bands may be attributed to the Raman-active vibrations of $Fe^{3+}O_6$ octahedral ionic groups in ilmenite (Wang *et al*. 2004).

The XRD pattern of Ti-rich magnetite in the Xinjie intrusion exhibits reflections corresponding to magnetite at *ca*. 2.96, 2.53, 2.09, 1.71, 1.61, and 1.48 Å, and relatively weak reflections corresponding to ilmenite at *ca*. 2.75, 2.23, 1.87, 1.50, 1.47, and 1.19 Å, respectively (Table 3). The XRD patterns of Ti-rich magnetite from the Bijigou and Panzhihua intrusions and the Damiao complex also exhibit several weak reflections, corresponding to spinel or Fe-rich spinel, at *ca*. 2.88, 2.45, 2.03, and 1.55 Å, respectively (Table 3). The cell parameters of the magnetite were determined using the d values of non-overlapping XRD reflections, *e.g.*, $d = \sim 2.42$ Å of the (222) reflection. In the Damiao complex and the Bijigou, Xinjie, and Panzhihua intrusion samples, the magnetite hosts have cell parameters (a_0) of 8.3882(3), 8.3979(9), 8.3911(6), 8.3924(7), and 8.3942(8) Å, respectively (Table 3), close to the a_0 value (8.396 Å) of pure magnetite (Wechsler *et al.* 1984). It is difficult to determine the exact cell parameters of the ilmenite lamellae (a_0 and c_0) due to weak X-ray reflections. The a_0 values of ilmenite exsolution are *ca*. 5.08 Å and the c_0 values are 14.08 Å (Table 3), also similar to pure ilmenite ($a_0 = 5.088$ Å, $c_0 = 14.092$ Å). The EMPA of the ilmenite lamellae are subject to the effects of neighboring minerals. Given that substitution of Fe^{3+} for Ti^{4+} would significantly decrease the cell parameters of ilmenite (Vincent *et al*. 1957, Basta 1959), the cell parameters of the $Ilmenite_{Xs}$ and $Ilmenite_{Xt}$

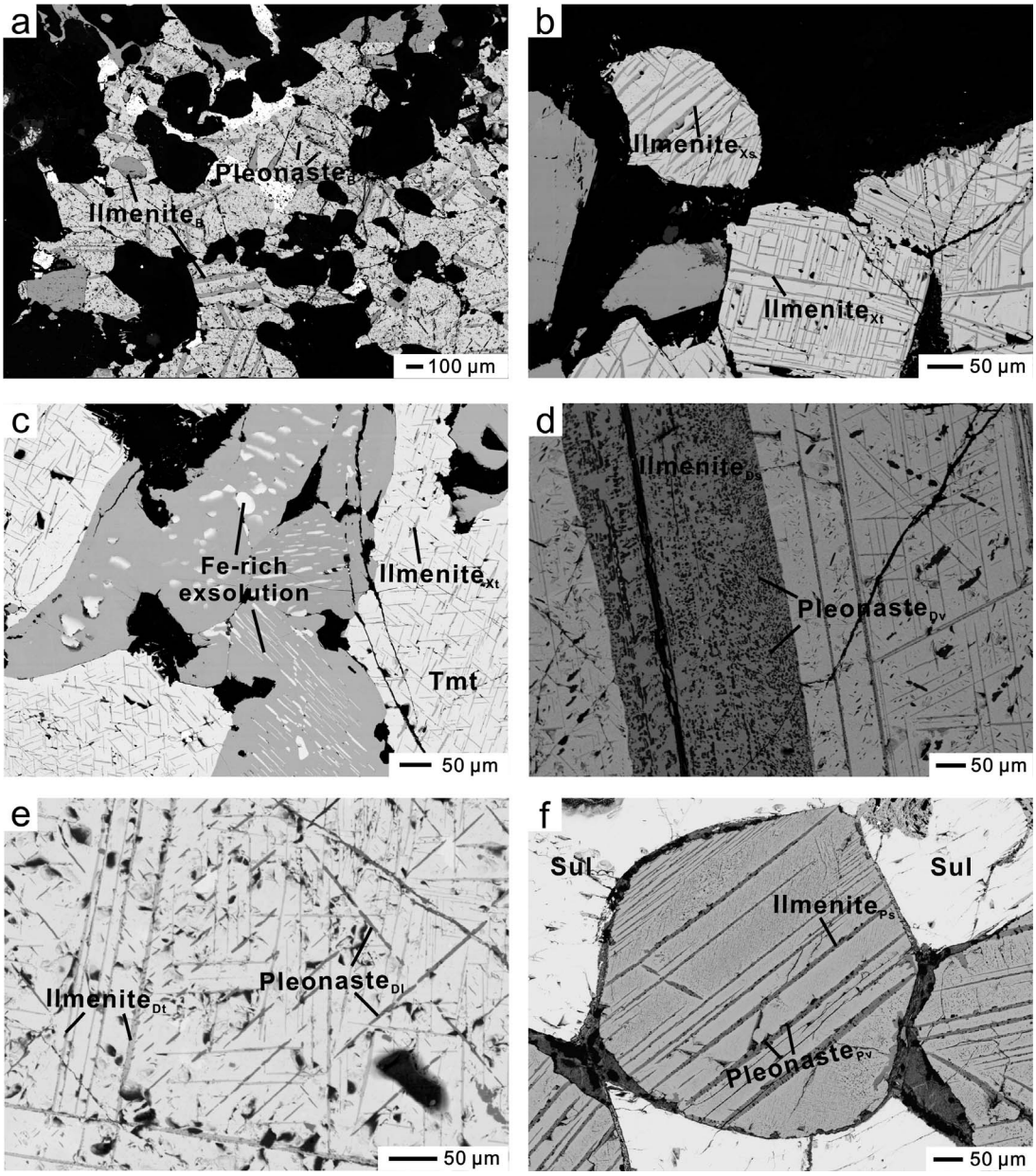

FIG. 1. BSE images of exsolution in Ti-rich magnetite from different magmatic intrusions. (a) Granule and thick ilmenite lamellae ($Ilmenite_B$) and pleonaste ($Pleonaste_B$) particles in the host magnetite, Bijigou intrusion. (b) Trellis-type ($Ilmenite_{Xt}$) and sandwich-type ($Ilmenite_{Xs}$) ilmenite lamellae lying along the {111} planes of the host magnetite, Xinjie intrusion. (c) Primary ilmenite grains hosting lamellae, granule-like, and oval-like Fe-rich exsolution and Ti-rich magnetite containing $Ilmenite_{Xt}$ lamellae, Xinjie intrusion. (d) Thick sandwich-type ilmenite ($Ilmenite_{Ds}$) lamellae (20 to 100 μm thick) in the host magnetite, and vermicular pleonaste ($Pleonaste_{Dv}$) particles in the $Ilmenite_{Ds}$ lamellae, Damiao complex. (e) Intergrowth of trellis-type ilmenite ($Ilmenite_{Dt}$) lamellae and pleonaste lamellae ($Pleonaste_{Dl}$), lying along the {111} and the {100} planes of the host magnetite respectively, Damiao complex. (f) Sandwich-type ilmenite ($Ilmenite_{Ps}$) in Ti-rich magnetite from the Panzhihua intrusion; note the vermicular pleonaste ($Pleonaste_{Pv}$) particles in the $Ilmenite_{Ps}$ lamellae and the interstitial sulfide (Sul) around the Ti-rich magnetite.

TABLE 1. COMPOSITIONS OF Ti-RICH MAGNETITE FROM DIFFERENT MAFIC-ULTRAMAFIC INTRUSIONS DETERMINED BY EMPA

	Bijigou		Damiao			Xinjie			Panzhihua				
Element (in wt.%)	Host magnetite	$Ilmenite_B$	Host magnetite	$Ilmenite_{Ds}$	$Ilmenite_{Dt}$	Host magnetite	$Ilmenite_{Xs}$	$Ilmenite_{Xt}$	Lamellae-poor zone (PZH-I)	Lamellae-rich zone (PZH-I)	$Ilmenite_{Ps}$ (PZH-I)	Lamellae-poor zone (PZH-II)	Lamellae-rich zone (PZH-II)
MgO	0.24	0.29	0.06	0.44	0.19	0.04	0.25	1.32	3.24	3.28	0.95	3.50	2.76
Al_2O_3	1.27	0.04	0.53	0.02	0.01	0.12	0.05	0.15	4.57	3.81	0.31	5.25	1.90
FeO_{total}	88.59	46.89	92.21	46.64	45.65	92.72	50.79	51.06	77.35	77.35	45.26	70.67	72.11
MnO	0.14	1.09	0.02	0.81	0.93	0.01	0.67	0.63	0.23	0.28	1.47	0.37	0.39
Cr_2O_3	0.10	0.01	0.21	0.03	0.08	0.05	0.02	0.03	0.03	0.00	0.00	0.01	0.02
V_2O_3	1.13	0.11	0.54	0.05	-	0.57	0.48	0.25	0.62	0.61	0.36	0.50	0.47
TiO_2	2.69	51.06	0.63	50.94	49.88	0.44	45.88	46.68	8.48	9.95	50.30	14.50	17.43
Total	94.15	99.50	94.20	98.92	96.87	93.94	98.15	100.11	98.73	99.47	98.65	94.80	95.07
$FeO_{cal.}$	34.06	44.34	32.06	45.84	44.90	31.72	40.23	39.05			45.25		
$Fe_2O_{3cal.}$	61.23	2.84	66.99	0.89	0.84	67.79	11.74	13.34			0.01		

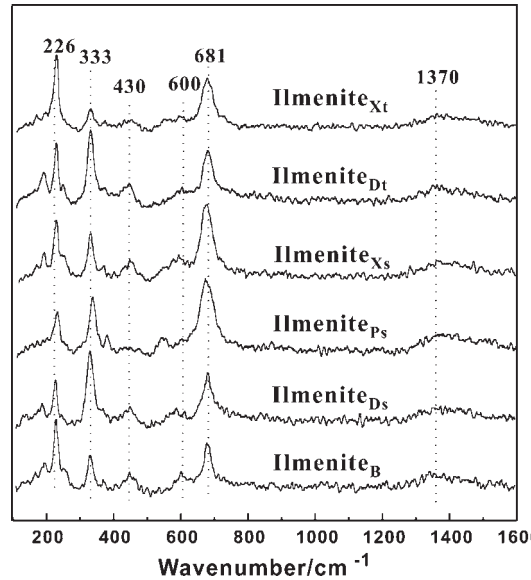

FIG. 2. Raman spectra of different types of ilmenite exsolution. $Ilmenite_B$, composite-type exsolution in the host magnetite of the Bijigou intrusion; $Ilmenite_{Ds}$, sandwich-type lamellae in the host magnetite of the Damiao complex; $Ilmenite_{Ps}$, sandwich-type lamellae in the host magnetite of the Panzhihua intrusion; $Ilmenite_{Xs}$, sandwich-type lamellae in the host magnetite of the Xinjie intrusion; $Ilmenite_{Dt}$, trellis-type lamellae in the host magnetite of the Damiao complex; $Ilmenite_{Xt}$, trellis-type lamellae in the host magnetite of the Xinjie intrusion.

lamellae suggest that their Fe_2O_3 content is less than 3 wt.%.

Ultrafine cloth-texture

The cloth texture shows ultrafine, discontinuous lamellae in the Ti-rich magnetite of the Panzhihua intrusion. The cloth-texture lamellae in the Ti-rich magnetite of the PZH-I sample, denoted as Cloth-I, exhibit different orientations with coexisting $Ilmenite_{Ps}$ lamellae (Fig. 3a). The cloth-texture lamellae in the Ti-rich magnetite of the PZH-II sample, denoted as Cloth-II, are parallel to the oriented lenticular pleonaste lamellae (Fig. 3b). The orientation of the cloth-texture lamellae indicates that they tend to align in the {100} rather than the {111} planes of the host magnetite. As the ultrafine lamellae are too small (less than 1 μm in width) to be directly characterized, identification of the ultrafine "cloth-texture" lamellae has been controversial (Vincent 1960, Price 1981, Vongruenewaldt *et al*. 1985, Speczik *et al*. 1988, Krasnova & Krezer 1995).

TABLE 2. RAMAN SHIFT REFERENCE OF STANDARD MINERALS

Minerals	Raman shift (cm^{-1})	Reference
Magnetite	670 540 308 193	Gasparov *et al.* (2000)
	667 539 305	Wang *et al.* (2004)
Ulvöspinel	680 561 497	
Ilmenite	683 368 333 207 224	
Hematite	1321* 613 497 411 301 292 245 226	

Note: __ represents strong and characteristic Raman bands of the mineral; * represents the broad band of hematite.

From BSE images, Ti-rich magnetite in the PZH-I and PZH-II samples contains two different zones with different cloth-texture lamellae density, *i.e.*, lamella-poor and lamella-rich zones (Fig. 3). The EMPA of the host magnetite of the PZH-I and PZH-II samples are also subject to the effect of the cloth-texture lamellae (Table 1). The lamella-poor zone of the PZH-I Ti-rich magnetite has 8.48 wt.% TiO_2, 4.57 wt.% Al_2O_3, and 3.24 wt.% MgO, and the lamella-rich zone has 9.95 wt.% TiO_2, 3.81 wt.% Al_2O_3, and 3.28 wt.% MgO. Similarly, the lamella-poor zone of PZH-II Ti-rich magnetite has 14.50 wt.% TiO_2, 5.25 wt.% Al_2O_3, and 3.50 wt.% MgO, and the lamella-rich zone has 17.43 wt.% TiO_2, 1.90 wt.% Al_2O_3, and 2.76 wt.% MgO (Table 1). It is noteworthy that the lamella-rich zones are richer in TiO_2 but poorer in Al_2O_3, while the lamella-poor zones are richer in Al_2O_3 and poorer in TiO_2. This suggests that the cloth-texture lamellae are composed of Ti-rich oxide minerals.

The Raman spectra of the lamella-rich zones in the PZH-I and PZH-II Ti-rich magnetites exhibit different features from magnetite (Fig. 4). Compared with the Raman bands of the host magnetite (nearly pure Fe_3O_4) in the sample from the Xinjie intrusion, the lamella-rich zones in the PZH-I and PZH-II Ti-rich magnetites exhibit a broadened band at ~673 cm^{-1} and two extra bands at ~230 cm^{-1} and ~333 cm^{-1}, corresponding to the Raman bands of ilmenite (Wang *et al*. 2004). The peak-fit analyses indicate that the broadened band can reasonably be viewed as an overlap of one band at ~668 cm^{-1} and another at ~685 cm^{-1}, corresponding to the indicative bands of magnetite and ilmenite, respectively (Wang *et al*. 2004). The indicative bands of ulvöspinel at 495 cm^{-1} and ~592 cm^{-1} (Wang *et al*. 2004, Zinin *et al*. 2011) are not shown in the Raman spectra.

The XRD patterns were obtained from ~0.01 mm^2 areas on the PZH-I and PZH-II Ti-rich magnetites. The XRD patterns exhibit sharp reflections of magnetite and relatively weak reflections of ilmenite, indicating that most of the cloth-texture lamellae are ilmenite. However, some reflections of magnetite are asymmetric and have shoulder peaks on the low-degree side, for example, the (400) reflection at ~43° (2θ) (Fig. 5). The shoulder of the (400) reflection can be reasonably viewed as an overlap of the (400) reflection and a weak one at ~42.35° (2θ) which corresponds to the (400) reflection of ulvöspinel. Although discernible reflections of ulvöspinel are not observed in both XRD patterns, the shoulders of some magnetite reflections suggest that the cloth-texture lamellae probably contain a small number of ulvöspinel relics.

Pleonaste exsolution

Four types of pleonaste exsolution were observed in this study, including droplet-like lamellae ($Pleonaste_B$) in Ti-rich magnetite from the Bijigou intrusion (Fig. 1a), vermicular pleonaste ($Pleonaste_{Dv}$ and $Pleonaste_{Pv}$) in the thick $Ilmenite_{Ds}$ lamellae (Fig. 1d) and the $Ilmenite_{Ps}$ lamellae (Fig. 3a), oriented lamellae ($Pleonaste_{Dl}$) in Ti-rich magnetite from the Damiao complex (Fig. 1e), and oriented lenticular pleonaste lamellae ($Pleonaste_{Pl}$) in the PZH-II Ti-rich magnetite (Fig. 3b). The exsolved pleonaste contains FeO, MgO, and Al_2O_3. The negative correlation of MgO and FeO (Fig. 6) and the R* ratio [$R^* = n_{Al3+} / (n_{Mg2+} + n_{Fe2+})$] of 2.0 (Table 4) indicate an isomorphous substitution between Fe^{2+} and Mg^{2+} in the pleonaste. The pleonaste exsolutions in different samples have variable $Mg^{\#}$ [$Mg^{\#} = n_{Mg2+} / (n_{Mg2+} + n_{Fe2+}) \times 100$] (Table 4), which are probably inherited from $spinel_{ss}$ precursors (Amcoff & Figueiredo 1990).

Iron-rich exsolution in primary ilmenite

Primary, euhedral to sub-euhedral ilmenite commonly crystallizes simultaneously with Ti-rich magnetite in both natural and synthetic processes (Buddington & Lindsley 1964). Multi-morphology exsolution, such as granule, oval, and oriented lamellae, are observed in primary ilmenite from different intrusions (Fig. 1c). The exsolved minerals were previously identified as magnetite or hematite based on optical/BSE images (Charlier *et al*. 2007,

TABLE 3. MICRO XRD ANALYTICAL RESULTS OF Ti-RICH MAGNETITE

Bijigou			Damiao			Xinjie											
Host Mag + Ilm + Ple			Host Mag + Ilm + Ple			Host Mag + Ilm			Host Ilm + Mag			Panzhihua (PHZ-I)			Panzhihua (PHZ-II)		
d (Å)	Height%	Phase	*d* (Å)	Height%	Phase	*d* (Å)	Height%	Phase	*d* (Å)	Height%	Phase	*d* (Å)	Height%	Phase	*d* (Å)	Height%	Phase
2.9726	10.50	Mag	2.9700	26.41	Mag	2.9653	30.03	Mag	2.9660	1.64	Mag	2.9707	43.24	Mag	2.9666	3.60	Mag
2.8784	0.87	Fe-rich Spn	2.7511	13.07	Ilm	2.7462	9.51	Ilm	2.7488	100.00	Ilm	2.8780	0.75	Spn	2.7466	4.18	Ilm
2.5461	42.96	Ilm	2.5367	65.60	Ilm	2.5440	37.62	Ilm	2.5297	8.21	Mag	2.7524	6.74	Ilm	2.5298	33.67	Mag
2.5356	100.00	Mag	2.5321	100.00	Mag	2.5300	100.00	Mag	2.2348	5.58	Ilm	2.5329	100	Mag	2.4457	1.77	Spn
2.4515	4.17	Fe-rich Spn	2.4513	3.97	Fe-rich Spn	2.4217	9.47	Mag	2.0968	3.48	Mag	2.4253	8.21	Mag	2.235	2.60	Ilm
2.4252	3.65	Mag	2.4249	14.95	Mag	2.2350	7.07	Ilm	1.8653	5.99	Ilm	2.3440	1.33	Ilm	2.0966	100	Mag
2.3459	1.45	Ilm	2.2348	3.72	Ilm	2.0964	17.07	Mag	1.7232	16.90	Ilm	2.0982	33.21	Mag	2.0324	0.44	Spn
2.1007	23.89	Mag	2.0966	18.58	Mag	1.8651	6.51	Ilm	1.6306	2.57	Ilm	1.8667	5.93	Ilm	1.8657	2.29	Ilm
1.8685	3.68	Ilm	1.8656	5.26	Ilm	1.7125	12.96	Mag	1.6150	2.41	Mag	1.7230	8.18	Ilm	1.7226	6.81	Ilm
1.7232	4.97	Ilm	1.7246	17.91	Ilm	1.6139	36.39	Mag	1.5042	5.13	Ilm	1.6204	24.58	Ilm	1.615	10.56	Mag
1.7111	7.51	Mag	1.7118	18.12	Mag	1.5033	7.13	Ilm	1.4837	4.17	Mag	1.6151	36.44	Mag	1.5553	0.43	Spn
1.6151	15.83	Mag	1.6139	56.13	Mag	1.4836	46.06	Mag	1.4668	2.62	Ilm	1.5517	1.82	Spn	1.5038	1.38	Ilm
1.5042	4.03	Ilm	1.5039	2.35	Ilm	1.4659	4.39	Ilm	1.1178	2.55	Ilm	1.5042	7.30	Ilm	1.4827	10.40	Mag
1.4837	32.94	Mag	1.4827	89.20	Mag	1.2650	6.41	Mag				1.4829	26.86	Mag	1.4667	1.30	Ilm
1.4695	3.35	Ilm	1.4672	4.50	Ilm	1.1192	5.75	Ilm				1.4658	2.64	Ilm			
1.2645	2.96	Mag	1.4474	3.30	Fe-rich Spn	1.0923	17.59	Mag				1.2651	6.23	Mag			
1.0966	2.13	Fe-rich Spn	1.2643	7.29	Mag												
1.0924	10.27	Mag	1.0916	19.65	Mag												
Mag-host a_0 = 8.3979(9) Å Ilm-lamellae a_0 = 5.08(1) Å c_0 = 14.09(1) Å			Mag-host a_0 = 8.3882(3) Å Ilm-lamellae a_0 = 5.08(1) Å c_0 = 14.09(1) Å			Mag-host a_0 = 8.3911(6) Å Ilm-lamellae a_0 = 5.08(1) Å c_0 = 14.07(1) Å			Ilm-host a_0 = 5.0849(4) Å c_0 = 14.067 (1) Å Mag-lamellae a_0 = 8.3940(8) Å			Mag-host a_0 = 8.3924(7) Å Ilm-lamellae a_0 = 5.082(4) Å c_0 =14.10(1) Å			Mag-host a_0 = 8.3942(8) Å Ilm-lamellae a_0 = 5.08(1) Å c_0 =14.07(1) Å		

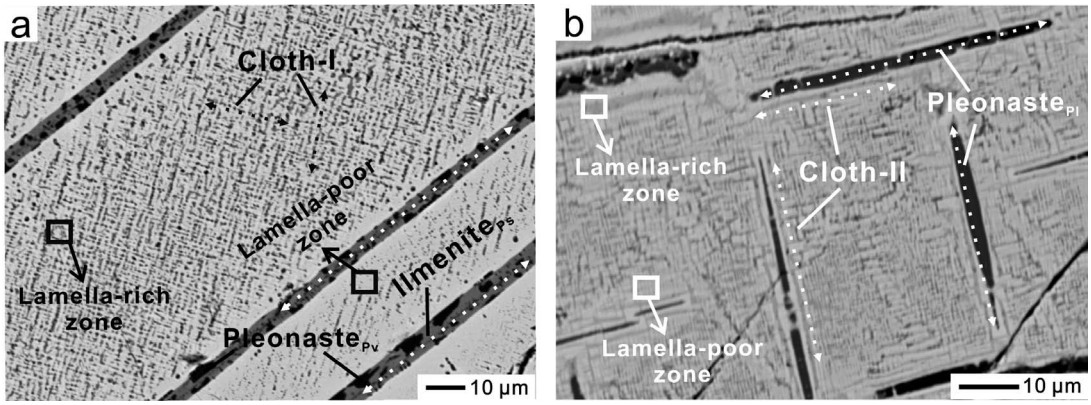

FIG. 3. BSE images of ultrafine cloth-texture lamellae in Ti-rich magnetite. (a) Ultrafine Cloth-I lamellae between the Ilmenite$_{Ps}$ lamellae in PZH-I Ti-rich magnetite. (b) Ultrafine Cloth-II lamellae among the oriented lenticular pleonaste lamellae (Pleonaste$_{Pl}$) in PZH-II Ti-rich magnetite; note the coarsened Cloth-II lamellae rimming the Pleonaste$_{Pl}$ lamellae.

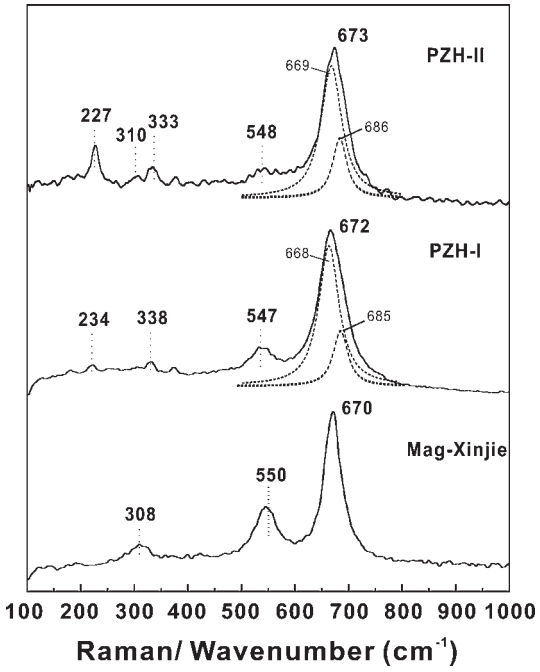

FIG. 4. Raman spectra collected from: Mag-Xinjie, host magnetite (nearly pure Fe_3O_4) in the sample from the Xinjie intrusion; PZH-I, the lamella-rich zone in PZH-I Ti-rich magnetite; PZH-II, the lamella-rich zone in PZH-II Ti-rich magnetite. Note that the main band at 672 cm^{-1} of PZH-I is an overlap of bands at 668 and 685 cm^{-1} (dashed line) and the main band at 673 cm^{-1} of PZH-II is an overlap of bands at 668 and 686 cm^{-1} (dashed line) based on analyses with PeakFit v4.12.

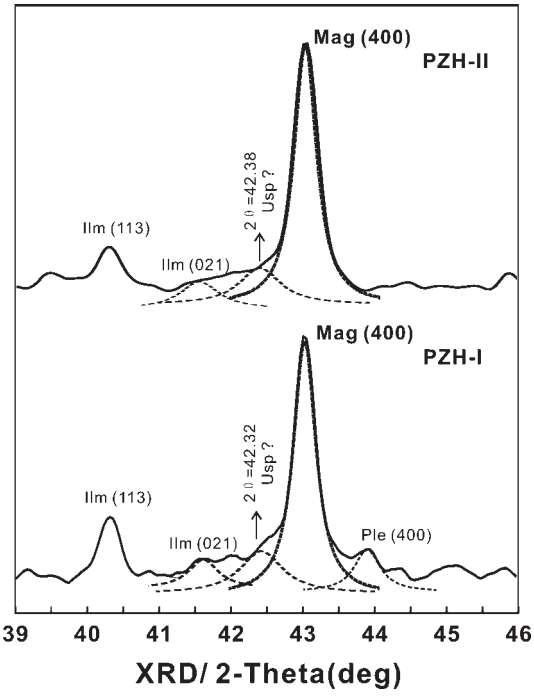

FIG. 5. Micro XRD patterns of PZH-I Ti-rich magnetite with Cloth-I lamellae and PZH-II Ti-rich magnetite with Cloth-II lamellae. Note that the (400) reflections of magnetite have shoulders corresponding to the (400) reflection of ulvöspinel at ~42.35° (2θ).

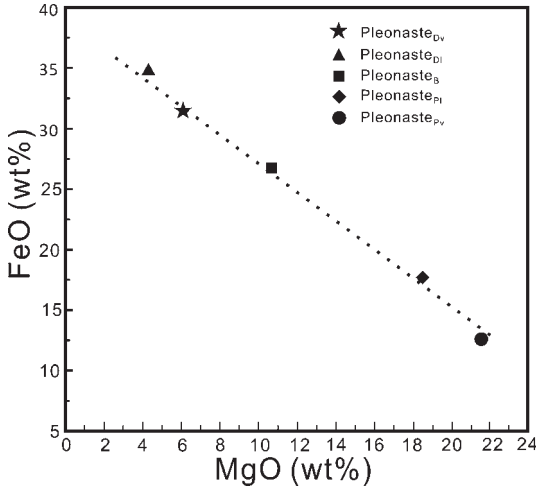

FIG. 6. A plot of MgO *versus* FeO for the different types of pleonaste in the Ti-rich magnetite of this study.

Pang *et al*. 2008, Wang *et al*. 2008, Morisset *et al*. 2010). However, the mineral identification is not convincing due to the lack of structural evidence.

The exsolved minerals contain up to ~90 wt.% FeO_{total} and 0.9 to 7 wt.% TiO_2 (Table 5). The XRD pattern of an ilmenite grain hosting the Fe-rich exsolution exhibits reflections of ilmenite and magnetite (Fig 7a). In addition, the Raman spectra of single granule or lamella of the Fe-rich exsolution exhibit typical bands of magnetite, including two strong bands at ~671 and ~554 cm^{-1} and a weak band at ~308 cm^{-1} (Fig 7b). The indicative vibrations of hematite are not shown in the Raman spectra. Accordingly, the exsolved minerals from the host ilmenite should be magnetite, rather than hematite. A reverse host-guest intergrowth of magnetite and ilmenite is found in the Xinjie intrusion in this study, *i.e*., primary Ti-rich magnetite hosts ilmenite exsolution, *versus* primary ilmenite hosting magnetite exsolution.

DISCUSSION

Interpretation of different intergrowths

$Spinel_{ss}$ contains significant amounts of Al^{3+}, Mg^{2+}, and Ti^{4+}. Different intergrowths of exsolved pleonaste and ilmenite may be formed due to the various bulk compositions of Ti-rich magnetite and different cooling history of the magmas (Price & Putnis 1979, Price 1980, Amcoff & Figueiredo 1990). Ilmenite exsolution can be formed by direct exsolution or "oxy-exsolution" at a wide range of temperatures (Buddington & Lindsley 1964, Lattard 1995). In contrast, exsolution of ulvöspinel and pleonaste in Ti-rich magnetite occurs at ~600 °C and ~900 °C, respectively (Vincent *et al*. 1957, Turnock & Eugster 1962, Buddington & Lindsley 1964). Hence, in different intergrowth relationships, the exsolution temperature of ilmenite can be constrained by coexisting ulvöspinel and pleonaste exsolution. On the other hand, exsolved pleonaste and ulvöspinel tend to align along the structurally favored {100} planes of host magnetite (Ramdohr 1953, Turnock & Eugster 1962, Price 1980, 1981), whereas exsolved ilmenite generally aligns along the {111} planes of host magnetite for crystal-structural reasons. Therefore, the orientation of exsolved pleonaste is helpful to distinguish the two exsolved titaniferous phases, ulvöspinel and ilmenite.

The Cloth-I lamellae exhibit different orientations from the $Ilmenite_{Ps}$ lamellae, and occur in the internal space of the $Ilmenite_{Ps}$ lamellae (Fig. 3a). The Cloth-II lamellae have the same orientation as the $Pleonaste_{Pl}$ lamellae and locally envelop the $Pleonaste_{Pl}$ lamellae

TABLE 4. COMPOSITIONS OF DIFFERENT TYPES OF PLEONASTE EXSOLUTION IN Ti-RICH MAGNETITE

Element (in wt.%)	$Pleonaste_B$	$Pleonaste_{Dv}$	$Pleonaste_{Dl}$	$Pleonaste_{Pv}$	$Pleonaste_{Pl}$
MgO	10.55	6.10	4.33	21.58	18.74
Al_2O_3	62.41	58.89	59.54	66.91	60.55
FeO_{total}	26.91	31.33	34.83	9.80	17.82
MnO	0.26	0.20	0.24	0.08	0.11
Cr_2O_3	0.06	0.48	0.34	0.01	0.010
V_2O_3	0.18	0.07	0.10	0.04	0.12
TiO_2	0.34	0.78	0.11	0.38	1.93
Total	100.70	97.84	99.48	98.79	99.28
$Mg^{\#}$	41.1	25.7	18.3	79.7	65.2
R*	2.0	2.0	2.0	2.0	1.8

Note: the $Mg^{\#} = n_{Mg2+} / (n_{Mg2+} + n_{Fe2+}) \times 100$; $R^* = n_{Al3+} / (n_{Mg2+} + n_{Fe2+})$

TABLE 5. COMPOSITIONS OF ILMENITE AND DIFFERENT TYPES OF FE-RICH EXSOLUTION

Element (in wt.%)	Host Ilmenite	Granule	Oval	Lamella
MgO	1.15	0.03	0.04	0.05
Al_2O_3	0.02	0.09	0.06	0.20
FeO_{total}	47.20	89.73	88.38	94.22
MnO	0.61	0.05	0.05	0
Cr_2O_3	0.02	0.06	0.05	0.12
V_2O_3	0.14	0.45	0.44	0.28
TiO_2	46.86	3.61	4.71	1.12
Total	96.01	94.02	93.72	95.99

(Fig. 3b). Such an intergrowth indicates that the cloth-texture lamellae align along the {100} rather than the {111} planes of the host magnetite, and that the cloth-texture lamellae occurred later than the coexisting $Ilmenite_{Ps}$ and $Pleonaste_{Pl}$ lamellae. The $Ilmenite_{Dt}$ lamellae and the $Pleonaste_{Dl}$ lamellae have different orientations, thus forming composite ilmenite-pleonaste trellises in the host magnetite (Fig. 1e). In this case, the $Ilmenite_{Dt}$ lamellae and $Pleonaste_{Dl}$ lamellae probably formed independently, parallel to the {100} and {111} planes of the host magnetite, respectively.

The occurrence of pleonaste–ilmenite symplectite in the Ti-rich magnetite from the Damiao complex ($Pleonaste_{Dv}$–$Ilmenite_{Ds}$, Fig. 1d) and Panzhihua intrusion ($Pleonaste_{Pv}$–$Ilmenite_{Ps}$, Fig. 3a) is noteworthy. Since Al_2O_3 would preferentially partition into magnetite rather than ilmenite (Sauerzapf *et al*. 2008), the pleonaste is unlikely to exsolve from the ilmenite lamellae. The irregular pleonaste particles and the ilmenite lamellae probably exsolved simultaneously from the $spinel_{ss}$, like a eutectoid crystallization process (Price & Putnis 1979, Amcoff & Figueiredo 1990, Elardo *et al*. 2012). In this case, the $Ilmenite_{Ds}$ lamellae formed at a temperature above or at least equal to the pleonaste–magnetite solvus at ~900 °C.

Exsolution-oxidation of ulvöspinel

Most Ti in $spinel_{ss}$ is in the form of Fe_2TiO_4 (Buddington & Lindsley 1964, Lattard 1995). The miscibility gap of $Usp–Mt_{ss}$ (< ~600 °C) would separate an ulvöspinel-rich phase from the $spinel_{ss}$ on slow cooling (Buddington & Lindsley 1964). The spinel-type structured ulvöspinel-rich phase tends to form lamellae along the {100} planes of the host magnetite (Ramdohr 1953, Price 1980, 1981). The orientation and morphology of the Cloth-I and Cloth-II lamellae indicate that they are ulvöspinel, whereas the Raman spectra and XRD patterns indicate that most of the cloth-texture lamellae are ilmenite. Given that ulvöspinel can only remain stable at extremely low oxygen fugacity and becomes unstable with decreasing temperature (Buddington & Lindsley 1964), such decoupling can be explained as the cloth-texture lamellae initially exsolving as ulvöspinel and becoming oxidized to ilmenite at a later stage, as in the reaction of Equation 1:

$$6Fe_2TiO_{4\ \text{ulvöspinel lamellae}} + O_2 = 6FeTiO_{3\ \text{cloth-texture lamellae}} + 2Fe_3O_{4\,\text{host}} \quad (1)$$

The oxidation may occur at very low temperature so that the ilmenite lamellae still align along the orientation of the ulvöspinel. In some cases, small amounts of ulvöspinel may remain as relics, as shown by the XRD patterns in this study (Fig. 5) and the previous study of Vincent (1960).

The ulvöspinel exsolution-oxidation process has been described as a "two-stage model" in previous studies (Verhoogen 1962, Vongruenewaldt *et al*. 1985,

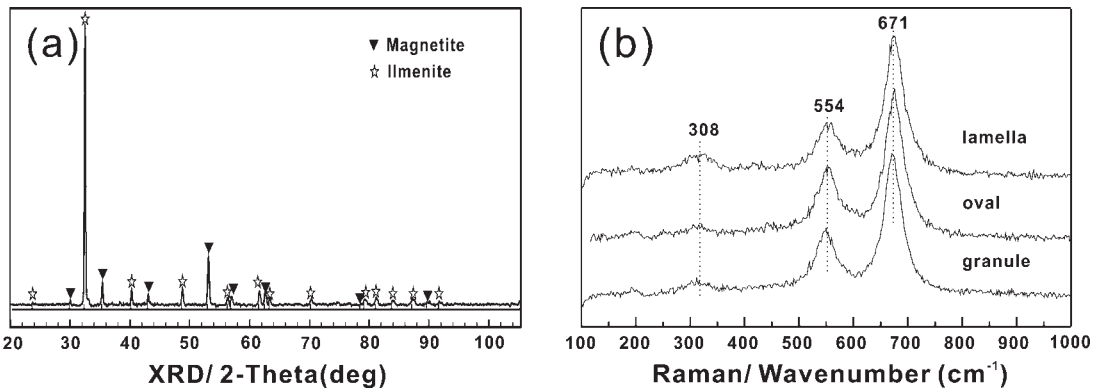

FIG. 7. (a) Micro XRD pattern of one primary ilmenite grain with Fe-rich exsolution. (b) Raman spectra of single lamella, oval-like, granule-like Fe-rich exsolution in the primary ilmenite grains of Figure 1c.

Pang *et al*. 2008). This process requires the $spinel_{ss}$ to remain at relatively reductive conditions until the temperature decreased to the magnetite–ulvöspinel solvus. The reductive conditions may have resulted from high contents of hydrogen or sulfur in the interstitial liquid or an excess of FeO relative to the fluids (Buddington & Lindsley 1964), which is consistent with the fact that the rocks in which the Ti-rich magnetite contains cloth-texture lamellae usually have high proportions of Fe-Ti oxides or sulfides.

"Oxy-exsolution" of ilmenite

Whether ulvöspinel or ilmenite is present as the exsolved phase in Ti-rich magnetite is mainly controlled by the oxidation–reduction equilibrium between $spinel_{ss}$ and fO_2. Under relatively oxidizing conditions, the Fe_2TiO_4 component in $spinel_{ss}$ could be oxidized at a temperature above the magnetite–ulvöspinel solvus and exsolved directly as ilmenite. This process was denoted as "oxy-exsolution" by Buddington & Lindsley (1964). The oxygen source is related to the reduction of coexisting silicate minerals and interstitial or trapped residual fluids (Frost 1991, Pang *et al*. 2008, Liu *et al*. 2014). The total amount of fluid is probably small relative to the Fe-Ti oxides in the bulk compositions of the whole rocks, however, the low proportion of fluids could cause large variations in fO_2 on cooling (Buddington & Lindsley 1964).

Note that the oxidation-reduction equilibrium is also dependent on temperature. For a given content of fluid (*e.g*., H_2O), Fe_2TiO_4-rich $spinel_{ss}$ may keep equilibrium with the fO_2 dominated by dissociation of liquid at high temperature, but tends to become unstable and oxidized with decreasing temperature (Buddington & Lindsley 1964). As a result, the $spinel_{ss}$ in equilibrium with the fluid tends to become successively lower in the Fe_2TiO_2 component, which becomes oxidized to ilmenite exsolution on cooling, as in the reaction of Equation 2:

$$6Fe_2TiO_{4\ \text{in spinel ss}} + O_2 = 6FeTiO_{3\ \text{trellis-/sandwich-type lamellae}} + 2Fe_3O_{4\,\text{host}} \quad (2)$$

The ilmenite lamellae tend to exsolve along the {111} planes of the host magnetite, whereas the generated magnetite becomes part of the host.

Under oxidizing conditions, if the host rock has a relatively high proportion of fluids, Fe_2TiO_4 in $spinel_{ss}$ tends to be exhausted by successive oxidations above the magnetite–ulvöspinel solvus. Compared with the Ti-rich magnetite in the massive ores, the cloth-texture lamellae are absent in the samples with minor Fe-Ti oxides, *e.g*., the samples from the Xinjie and Bijigou intrusions. In these samples, most of the Fe_2TiO_4 component in the $spinel_{ss}$ exsolves as ilmenite lamellae by the "oxy-exsolution" process and the host mineral becomes nearly pure magnetite.

Direct exsolution of ilmenite

The ilmenite lamellae in Ti-rich magnetite are also possibly formed by direct exsolution from cation-deficient $spinel_{ss}$ (Lattard 1995). Cation-deficient $spinel_{ss}$ was previously regarded as "titanomaghemite", which is formed by an oxidation process analogous to the formation of maghemite (γ-Fe_2O_3) (Basta 1959, Collyer *et al*. 1988, Zhou *et al*. 1999). However, synthetic experiments indicate that cation-deficient $spinel_{ss}$ can also be formed by the substitution of Fe^{2+} by Ti^{4+}, as in Equation 3:

$$2Fe^{2+} = \square + Ti^{4+} \quad (3)$$

at low fO_2 and high-temperature conditions. The cation-deficient $spinel_{ss}$ can be considered as a solid solution within the Fe_2TiO_4–Fe_3O_4–γ-$FeTiO_3$ system. Substitution of Fe^{2+} by other high valence cations, such as Al^{3+} and Cr^{3+}, as in Equation 4:

$$3Fe^{2+} = \square + 2X\,(X = Fe^{3+}, Cr^{3+}, Al^{3+}, \text{and } V^{3+}) \quad (4)$$

can also increase the vacancy concentration of $spinel_{ss}$ (Lattard 1995). Vacancy relaxation would occur in a cooling process from the crystallization temperature to 900 °C, and the cation-deficient $spinel_{ss}$ would become stoichiometric by exsolving ilmenite (Lattard 1995).

Given the low concerntrations of vacancies (or excess Ti^{4+}) in the cation-deficient $spinel_{ss}$ (Lattard 1995), limited amounts of ilmenite lamellae are expected to form by direct exsolution. The maximum amount of vacancies in the place of cations in $spinel_{ss}$ is ~2% at 1300 °C (Taylor 1964). Calculations using the Lever Rule and Taylor's data suggest that the maximum amount of ilmenite that could be formed by direct exsolution makes up ~15 wt.% or ~16% vol.% of the whole Ti-rich magnetite crystal.

In most terrestrial rocks, ilmenite exsolution in Ti-rich magnetite is commonly formed by the "oxy-exsolution" process (Lattard 1995). As high pressure seems to lower vacancy contents in $spinel_{ss}$ (Lattard 1995), the amount of ilmenite formed by direct exsolution in the Ti-rich magnetite from intrusions is probably less than the above estimation. However, in this study, some ilmenite exsolution is suggested to be formed by direct exsolution of cation-deficient $spinel_{ss}$. The broad sandwich-type $Ilmenite_{Ps}$ lamellae make up 7–11 vol.% of the total Ti-rich magnetite based on modal analysis (Fig. 3a). The $Pleonaste_{Pv}$–

$Ilmenite_{Ps}$ symplectite suggests $Ilmenite_{Ps}$ lamellae formed at temperatures above 900 °C, whereas the coexisting Cloth-I lamellae indicates that the $spinel_{ss}$ remained un-oxidized under relatively reduced conditions above the magnetite–ulvöspinel solvus (~600 °C). Thus the $Ilmenite_{Ps}$ lamellae are likely formed by direct exsolution from a cation-deficient $spinel_{ss}$.

Inter-oxide re-equilibration

$Spinel_{ss}$ and $Ilm–Hem_{ss}$ can crystallize simultaneously from magmas at a wide range of oxygen fugacities and temperatures (Buddington & Lindsley 1964). For $Ilm–Hem_{ss}$, a miscibility gap would separate a hematite-rich phase from an ilmenite-rich phase on cooling (Lindsley 1991), and the ilmenite in many mafic-ultramafic intrusions thus contains hematite exsolutions (McEnroe *et al*. 2002, Kasama *et al*. 2009, Morisset *et al*. 2010). Magnetite exsolution, which cannot be formed by isochemical decomposition of $Ilm–Hem_{ss}$, also occurs in the host ilmenite in some intrusions, such as Xinjie. In the "oxy-exsolution" model (Buddington & Lindsley 1964), the magnetite exsolution is considered to be a reductive product of the Fe_2O_3 component in $Ilm–Hem_{ss}$ with decreasing fO_2, as in the reaction of Equation 5:

$$6Fe_2O_{3\ \text{in Ilm–Hem ss}} = 4Fe_3O_{4\,\text{exsolution}} + O_2 \qquad (5)$$

However, note that ilmenite lamellae formed by sub-solidus oxidation with increasing fO_2 also occur in the coexisting Ti-rich magnetite (Fig. 1c). Thus the reversed host-guest intergrowth is unlikely to be derived from fO_2 fluctuation controlled by fluids or coexisting silicate minerals. In the sample of the present study, Fe-Ti oxides are dominant. The cooling path of the oxide assemblage is more likely controlled by sub-solidus cation re-equilibration between coexisting Ti-rich magnetite and ilmenite (Frost 1991). In this case, the reversed host-guest intergrowth likely formed under oxygen-conserving conditions. Simultaneous oxidation and reduction can occur by cation re-equilibration, as shown by Equation 6, with no change in the oxygen content of the oxide assemblage.

A similar intergrowth was also reported in the synthetic experiment (Lattard 1995), which is attributed to a combined function of vacancy relaxation and cation exchange $Fe^{2+}TiFe^{3+}_{-2}$ between coexisting $Ilm–Hem_{ss}$ and $spinel_{ss}$:

$$\begin{aligned} Fe_2TiO_{4\ \text{in spinel ss}} + Fe_2O_{3\ \text{in Ilm–Hem ss}} \\ = FeTiO_{3\ \text{exsolution in magnetite host}} \\ + Fe_3O_{4\ \text{exsolution in ilmenite host}} \end{aligned} \qquad (6)$$

The cation exchange can occur at temperatures above the solvus of $Ilm–Hem_{ss}$ and $spinel_{ss}$ and proceeds to the right on cooling. As a result, the $spinel_{ss}$ gains Fe^{3+} and the $Ilm–Hem_{ss}$ loses a corresponding amount of Fe^{3+}. Both $Ilm–Hem_{ss}$ and $spinel_{ss}$ would approach their endmember compositions in the process (Frost 1991). Because Fe^{2+} has higher octahedral site preference energy than Ti^{4+}, and more preferentially occupies the octahedral site of $Ilm–Hem_{ss}$ (Dunitz & Orgel 1957, O'Neill & Navrotsky 1983), the diffusion of Fe^{2+} from the $spinel_{ss}$ to the $Ilm–Hem_{ss}$ is likely faster than that of Ti^{4+} from the $Ilm–Hem_{ss}$ to the $spinel_{ss}$. Therefore, the diffused Fe^{2+} from $spinel_{ss}$ and the diffused Fe^{3+} from $Ilm–Hem_{ss}$ can precipitate in the form of magnetite within the ilmenite host, whereas the Fe_2TiO_4 component in $spinel_{ss}$ exsolves to form ilmenite lamellae with Fe^{2+} diffusing to coexisting $Ilm–Hem_{ss}$.

Petrologic implications

Titanium-rich magnetite in the rocks of the intrusive bodies commonly experienced intensive sub-solidus re-equilibration on slow cooling (Frost 1991). Sub-solidus oxidation plays a key role in the transformation of the Fe_2TiO_4 component in $spinel_{ss}$ to the ilmenite exsolution in Ti-rich magnetite. In most cases, the ilmenite exsolution in the Ti-rich magnetite formed by the "exsolution-oxidation" and "oxy-exsolution" processes (Buddington & Lindsley 1964, Lattard 1995). Compared with the original composition of the $spinel_{ss}$, the Fe^{3+}/Fe^{2+} ratio of the Ti-rich magnetite is significantly increased by the oxidation processes, whereas the Fe/Ti ratio of the Ti-rich magnetite remains the same. In this case, the original Fe^{3+}/Fe^{2+} ratio of the $spinel_{ss}$ can be obtained by partitioning FeO_{total} of the Ti-rich magnetite (including ilmenite exsolution) according to the formula of stoichiometric $spinel_{ss}$.

The ilmenite exsolution formed by the "oxy-exsolution" process often exhibits progressive variations in terms of size and morphology with oxidation status and temperature (Fig. 1b). In this study, the Ti-rich magnetite in some samples is noted to contain two distinctive generations of ilmenite lamellae, probably representing two stages of ilmenite formation (Fig. 8). One of the two generations of ilmenite lamellae may have formed by direct exsolution or inter-oxide re-equilibration rather than the "oxy-exsolution" process. For example, the coarse $Ilmenite_{Xs}$ lamellae coexisting with ultrafine $Ilmenite_{Xt}$ lamellae (Fig. 8a) probably formed by direct exsolution at high temperature, and the lenticular ilmenite lamellae coexisting with $Ilmenite_{Xt}$ lamellae (Fig. 8b) may have resulted from inter-oxide re-equilibration, as evidenced by the close intergrowth of Ti-rich magnetite and primary ilmenite.

The ilmenite exsolution formed by direct exsolution should be considered as the γ-$FeTiO_3$ component

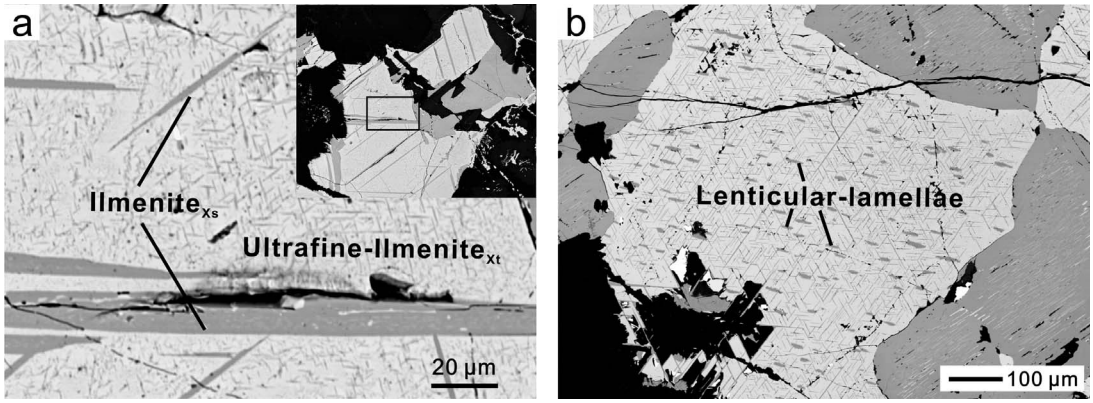

FIG. 8. BSE images of Ti-rich magnetite with two generations of ilmenite exsolution: (a) Intergrowth of coarse Ilmenite$_{Xs}$ lamellae and ultrafine Ilmenite$_{Xt}$ lamellae; (b) Intergrowth of lenticular ilmenite lamellae and Ilmenite$_{Xt}$ lamellae.

of the original spinel$_{ss}$, and the minor amount of vacancy and excess Ti must thus be taken into consideration in the usage of the Ti-rich magnetite-ilmenite thermo-oxybarometer (Lattard 2005), as the small variations in the Fe/Ti and Fe^{3+}/Fe^{2+} ratios of the original spinel$_{ss}$ may lead to significant changes in calculated temperature and fO_2 (Buddington & Lindsley 1964, Lattard *et al*. 1995). On the other hand, the inter-oxide re-equilibration enhances the ilmenite exsolution due to the diffusion of Fe^{2+} from Ti-rich magnetite to adjacent ilmenite, and such a process decreases the Fe/Ti and Fe^{2+}/Fe^{3+} ratios of the Ti-rich magnetite. The loss of Fe^{2+} in Ti-rich magnetite by inter-oxide re-equilibration should be estimated by the amounts of magnetite exsolution in the adjacent ilmenite and added to the original composition of the spinel$_{ss}$.

ACKNOWLEDGMENTS

This is contribution no. IS-2151 from GIG CAS. We are grateful to Xiangping Gu at the Central South University in China for the micro XRD analysis. Taiping Zhao kindly provided the samples from the Damiao complex. This work was financially supported by NSFC grants No.41172045 and 41325006, and CAS/SAFEA IPP for CRT project 20140491534. Critical and constructive comments from Prof. Donald H. Lindsley and an anonymous reviewer are appreciated.

REFERENCES

AMCOFF, O. & FIGUEIREDO, B.R. (1990) Mechanisms of Retrograde Changes in oxide minerals from the Proterozoic Serrote Da Laje deposit, Northeastern Brazil. *Mineralium Deposita* **25**, 313–322.

BASTA, E.Z. (1959) Some mineralogical relationships in the system Fe_2O_3–Fe_3O_4 and the composition of titanomaghemite. *Economic Geology* **54**, 698–719.

BUDDINGTON, A.F. & LINDSLEY, D.H. (1964) Iron-Titanium oxide minerals and synthetic equivalents. *Journal of Petrology* **5**, 310–357.

CHARLIER, B., SKÅR, Ø., KORNELIUSSEN, A., DUCHESNE, J.C., & VANDER, A.J. (2007) Ilmenite composition in the Tellnes Fe-Ti deposit, SW Norway: fractional crystallization, postcumulus evolution and ilmenite-zircon relation. *Contributions to Mineralogy and Petrology* **154**, 119–134.

CHEN, W.T., ZHOU, M.F., & ZHAO, T.P. (2013) Differentiation of nelsonitic magmas in the formation of the ~1.74 Ga Damiao Fe-Ti-P ore deposit, North China. *Contributions to Mineralogy and Petrology* **165**, 1341–1362.

COLLYER, S., GRIMES, N.W., VAUGHAN, D.J., & LONGWORTH, G. (1988) Studies of the crystal-structure and crystal-chemistry of titanomaghemite. *American Mineralogist* **73**, 153–160.

DÉGI, J., ABART, R., TÖRÖK, K., BALI, E., WIRTH, R., & RHEDE, D. (2010) Symplectite formation during decompression induced garnet breakdown in lower crustal mafic granulite xenoliths: mechanisms and rates. *Contributions to Mineralogy and Petrology* **159**, 293–314.

DIECKMANN, R. (1982) Defects and cation diffusion in magnetite (IV): nonstoichiometry and point defect structure of magnetite ($Fe_{3-\delta}O_4$). *Berichte der Bunsengesellschaft für physikalische Chemie* **86**, 112–118.

DONG, H., XING, C.M., & WANG, C.Y. (2013) Textures and mineral compositions of the Xinjie layered intrusion, SW China: implications for the origin of magnetite and fractionation process of Fe-Ti-rich basaltic magmas. *Geoscience Frontiers* **4**, 503–515.

Dunitz, J.T. & Orgel, L. (1957) Electronic properties of transition-metal oxides-II: Cation distribution amongst octahedral and tetrahedral sites. *Journal of Physics and Chemistry of Solids* **3**, 318–323.

Elardo, S.M., McCubbin, F.M., & Shearer, C.K. (2012) Chromite symplectites in Mg-suite troctolite 76535 as evidence for infiltration metasomatism of a lunar layered intrusion. *Geochimica et Cosmochimica Acta* **87**, 154–177.

Frost, B.R. (1991) Introduction to oxygen fugacity and its petrologic importance. *In* Oxide minerals: petrologic and magnetic significance (D.H. Lindsley, ed.). *Reviews in Mineralogy and Geochemistry* **25**, 1–9.

Frost, B.R. (1991) Magnetic petrology: factors that control the occurrence of magnetite in crustal rocks. *Reviews in Mineralogy and Geochemistry* **25**, 489–509.

Frost, B.R. & Lindsley, D.H. (1991) Occurrence of iron-titanium oxides in igneous rocks. *In* Oxide minerals: petrologic and magnetic significance (D.H. Lindsley, ed.). *Reviews in Mineralogy and Geochemistry* **25**, 433–468.

Gasparov, L.V., Tanner, D.B., Romero, D.B., Berger, H., Margaritondo, G., & Forro, L. (2000) Infrared and Raman studies of the Verwey transition in magnetite. *Physical Review B* **62**, 7939–7944.

Haggerty, S.E. (1991) Oxide textures, a mini-atlas. *Reviews in Mineralogy and Geochemistry* **25**, 129–219.

Kasama, T., Dunin-Borkowski, R.E., Asaka, T., Harrison, R.J., Chong, R.K., McEnroe, S.A., Simpson, E.T., Matsui, Y., & Putnis, A. (2009) The application of Lorentz transmission electron microscopy to the study of lamellar magnetism in hematite-ilmenite. *American Mineralogist* **94**, 262–269.

Krasnova, N.I. & Krezer, Y.L. (1995) New data on the nature of fine and ultrafine lamellae in titanomagnetite. *European Journal of Mineralogy* **7**, 1361–1372.

Lattard, D. (1995) Experimental evidence for the exsolution of ilmenite from titaniferous spinel. *American Mineralogist* **80**, 968–981.

Lattard, D., Sauerzapf, U., & Kasemann, M. (2005) New calibration data for the Fe-Ti oxide thermo-oxybarometers from experiments in the Fe–Ti–O system at 1 bar, 1000–1300 °C and a large range of oxygen fugacities. *Contributions to Mineralogy and Petrology* **149**, 735–754.

Lindsley, D.H. (1963) Equilibrium relations of coexisting pairs of Fe-Ti oxides. *Carnegie Institution of Washington Year Book* **62**, 60–66.

Lindsley, D.H. (1991) Experimental studies of oxide minerals. *Reviews in Mineralogy and Geochemistry* **25**, 69–106.

Liu, P.P., Zhou, M.F., Chen, W.T., Boone, M., & Cnudde, V. (2014) Using Multiphase Solid Inclusions to Constrain the Origin of the Baima Fe–Ti–(V) Oxide Deposit, SW China. *Journal of Petrology* **55**, 951–976.

Liu, P.P., Zhou, M.F., Chen, W.T., Gao, J.F., & Huang, X.W. (2015) *In-situ* LA-ICP-MS trace elemental analyses of magnetite: Fe–Ti–(V) oxide-bearing mafic–ultramafic layered intrusions of the Emeishan Large Igneous Province, SW China. *Ore Geology Reviews* **65**, 853–871.

Mücke, A. (2003) Magnetite, ilmenite and ulvite in rocks and ore deposits: petrography, microprobe analyses and genetic implications. *Mineralogy and Petrology* **77**, 215–234.

McConnell, J. (1975) Microstructures of minerals as petrogenetic indicators. *Annual Review of Earth and Planetary Sciences* **3**, 129–155.

McEnroe, S., Harrison, R., Robinson, P., & Langenhorst, F. (2002) Nanoscale haematite–ilmenite lamellae in massive ilmenite rock: an example of 'lamellar magnetism' with implications for planetary magnetic anomalies. *Geophysical Journal International* **151**, 890–912.

Morisset, C.E., Scoates, J.S., Weis, D., Sauve, M., & Stanaway, K.J. (2010) Rutile-Bearing ilmenite deposits associated with the Proterozoic Saint-Urbain and Lac Allard Anorthosite Massifs, Grenville Province, Quebec. *Canadian Mineralogist* **48**, 821–849.

O'Neill, H.S.C. & Navrotsky, A. (1983) Simple spinels; crystallographic parameters, cation radii, lattice energies, and cation distribution. *American Mineralogist* **68**, 181–194.

Pang, K.N., Zhou, M.F., Lindsley, D., Zhao D.G., & Malpas, J. (2008) Origin of Fe-Ti oxide ores in mafic intrusions: evidence from the Panzhihua intrusion, SW China. *Journal of Petrology* **49**, 295–313.

Pang, K.N., Zhou, M.F., Qi, L., Shellnutt, G., Wang, C.Y., & Zhao, D.G. (2010) Flood basalt-related Fe–Ti oxide deposits in the Emeishan large igneous province, SW China. *Lithos* **119**, 123–136.

Price, G.D. (1980) Exsolution microstructures in titanomagnetite and their magnetic significance. *Physics of the Earth and Planetary Interiors* **23**, 2–12.

Price, G.D. (1981) Subsolidus phase relations in the titanomagnetite solid solution series. *American Mineralogist* **66**, 751–758.

Price, G.D. & Putnits, A. (1979) Oxidation phenomena in pleonaste bearing titanomagnetite. *Contributions to Mineralogy and Petrology* **69**, 355–359

Ramdohr, P. (1953) Ulvöspinel and its significance in titaniferous iron ores. *Economic Geology* **48**, 677–688.

Ramdohr, P. (1980) *The ore minerals and their intergrowth*, 2nd Edition. International series in earth science, Academic Press, New York, United States.

Reynolds, I.M. (1985) Contrasted mineralogy and textural relationships in the uppermost titaniferous magnetite

layers of the Bushveld Complex in the Bierkraal area north of Rustenburg. *Economic Geology* **80**, 1027–1048.

Sauerzapf, U., Lattard, D., Burchard, M., & Engelmann, R. (2008) The titanomagnetite–ilmenite equilibrium: new experimental data and thermo-oxybarometric application to the crystallization of basic to intermediate rocks. *Journal of Petrology* **49**, 1161–1185.

Senderov, E., Dogan, A.U., & Navrotsky, A. (1993) Nonstoichiometry of magnetite-ulvöspinel solid solutions quenched from 1300 degrees C. *American Mineralogist* **78**, 565–573.

Shebanova, O.N. & Lazor, P. (2003) Raman study of magnetite (Fe_3O_4): laser-induced thermal effects and oxidation. *Journal of Raman Spectroscopy* **34**, 845–852.

Song, X.Y., Qi, H.W., Hu, R.Z., Chen, L.M., Yu, S.Y., & Zhang, J.F. (2013) Formation of thick stratiform Fe-Ti oxide layers in layered intrusion and frequent replenishment of fractionated mafic magma: Evidence from the Panzhihua intrusion, SW China. *Geochemistry Geophysics Geosystems* **14**, 712–732.

Speczik, S., Wiszniewska, J., & Diedel, R. (1988) Minerals, exsolution features and geochemistry of Fe-Ti ores of the Suwalki-District (Northeast Poland). *Mineralium Deposita* **23**, 200–210.

Spencer, K.J. & Lindsley, D.H. (1981) A solution model for coexisting iron-titanium oxides. *American Mineralogist* **66**, 1189–1201.

Turnock, A. & Eugster, H. (1962) Fe-Al Oxides: phase relationships below 1000 °C. *Journal of Petrology* **3**, 533–565.

Verhoogen, J. (1962) Oxidation of iron-titanium oxides in igneous rocks. *The Journal of Geology* **70**, 168–181.

Vincent, E. (1960) Ulvöspinel in the skaergaard intrusion, East Greenland. *Neues Jahrbuch für Mineralogie - Abhandlungen* **94**, 992–1016.

Vincent, E., Wright, J., Chevallier, R., & Mathieu, S. (1957) Heating experiments on some natural titaniferous magnetite. *Mineralogical Magazine* **31**, 624–655.

Vongruenewaldt, G., Klemm, D.D., Henckel, J., & Dehm, R.M. (1985) Exsolution features in titanomagnetite from massive magnetite layers and their host rocks of the upper zone, eastern Bushveld Complex. *Economic Geology* **80**, 1049–1061.

Wang, A., Kuebler K.E., Jolliff, B.L., & Haskin L.A. (2004) Raman spectroscopy of Fe-Ti-Cr-oxides, case study: martian meteorite EETA79001. *American Mineralogist* **89**, 665–680.

Wang, C.Y., Zhou, M.F., & Zhao, D.G. (2008) Fe-Ti-Cr oxides from the Permian Xinjie mafic-ultramafic layered intrusion in the Emeishan large igneous province, SW China: crystallization from Fe- and Ti-rich basaltic magmas. *Lithos* **102**, 198–217.

Zhou, W., Peacor, D.R., Van, D.V.R., & Mansfield, J.F. (1999) Determination of lattice parameter, oxidation state, and composition of individual titanomagnetite/titanomaghemite grains by transmission electron microscopy. *Journal of Geophysical Research: Solid Earth (1978–2012)* **104**, 17689–17702.

Zhou, M.F., Kennedy, A.K., Sun, M., Malpas, J., & Lesher, C.M. (2002) Neoproterozoic arc-related mafic intrusions along the northern margin of South China: implications for the accretion of Rodinia. *The Journal of Geology* **110**, 611–618.

Zhou, M.F., Robinson, P.T., Lesher, C.M., Keays, R.R., Zhang, C.J., & Malpas, J. (2005) Geochemistry, petrogenesis and metallogenesis of the Panzhihua gabbroic layered intrusion and associated Fe-Ti-V oxide deposits, Sichuan Province, SW China. *Journal of Petrology* **46**, 2253–2280.

Zinin, P., Tatsumi-Petrochilos, L., Bonal, L., Acosta, T., Hammer, J., Gilder, S., & Fuller, M. (2011) Raman spectroscopy of titanomagnetite: calibration of the intensity of Raman peaks as a sensitive indicator for their Ti content. *American Mineralogist* **96**, 1537–1546.

Received September 10, 2014. Revised manuscript accepted October 22, 2015.